

The effect of hydrolysis duration on the phase composition, texture, aggregation and agglomeration of ZrO₂ nanoparticles

Sh. O. Omarov

Ioffe Institute, Saint Petersburg, 194021, Russia

somarov@mail.ioffe.ru

PACS 81.20.-n, 61.46.+w, 81.10.-h, 64.70K

DOI 10.17586/2220-8054-2021-12-4-472-480

In this work, a number of ZrO₂ · nH₂O and ZrO₂ samples were synthesized by direct precipitation and hydrolysis with different duration (36 and 61 h) followed by neutralization and thermal treatment. The prepared samples were analyzed using DT-TGA, PXRD, N₂ physisorption and LD methods. The dependence of the size of crystallites and secondary particles, phase composition, texture, and particle morphology on the amount of zirconium hydrolyzed to form *m*-ZrO₂ is shown. The possibility of regulating the phase composition of ZrO₂ has been established while maintaining the specific surface area (110 – 120 m²/g), as well as creating a hierarchical system of micro-mesopores. The mechanism of the ZrO₂ · nH₂O formation during hydrolysis and precipitation is considered. The size of the critical nucleus is estimated (1.5 – 2 nm).

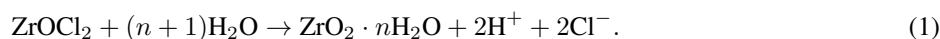
Keywords: zirconia, hydrolysis, phase composition, texture, aggregation, agglomeration, mechanism.

Received: 18 July 2018

1. Introduction

Zirconia has found application in the production of ceramic and catalysts, incl. those used in industrial applications [1–3]. It is considered that the tetragonal modification of ZrO₂ (*t*-ZrO₂) is preferable because it has a better porous structure, developed surface acidity, and defective structure. It was however shown [4, 5] that catalysts based on the monoclinic modification (*m*-ZrO₂) are more active but less stable by time on stream. Therefore, it is urgent to study in detail the possibility of obtaining *m*-ZrO₂ with a more developed porous structure and to study the possibility of obtaining and controlling the *t*-ZrO₂/*m*-ZrO₂ ratio.

Precipitation from aqueous solutions of salts is the main method for the synthesis of ZrO₂, during which nanosized X-ray amorphous hydrous zirconia (ZrO₂ · nH₂O) is formed. This is an effective method for the preparation of *t*-ZrO₂ nanocrystallites with a developed mesoporous structure, which is formed during thermal treatment at 350 – 450 °C. There are other methods: hydrolysis of aqueous solutions of salts [6–9], hydrothermal treatment [10], solution combustion [11], thermal decomposition of salts [12], heterophase conversion [13], etc. Matsui et al. [6–9] showed that a sol consisting of *m*-ZrO₂ nanoparticles (crystallites 2.2 – 4.9 nm, agglomerates 100 – 200 nm) is formed upon the long-term maintenance of a ZrOCl₂ solution at 100 °C during complete hydrolysis of the salt. The hydrolysis reaction proceeded as follows:



This method makes it possible to obtain phase-purified *m*-ZrO₂. However, the results on the porous structure are absent in the listed works, and in [5] and other similar studies, only the value of the specific surface area is given. Salt concentration, temperature and duration of hydrolysis are the most important parameters of synthesis [9]. Extraneous cations (Al³⁺, Ca²⁺) have no effect [7], while the presence of HCl, NaCl, NH₄OH allows regulation of the rate and completeness of hydrolysis, crystallite size and agglomerates of *m*-ZrO₂ due to a decrease in the effect of the electric double layer and an increase in heterocoagulation [6–8]. However, the intermediate states remained unexplored, when only a part of the primary forms of zirconium passed into the sol during complete hydrolysis. The residual solution can be neutralized with a base solution, thus allowing the phase composition of ZrO₂ to be adjusted.

In this work, the effect of the hydrolysis duration of a ZrOCl₂ solution, additionally neutralized with an NH₄OH solution, on the structural and morphological properties of ZrO₂ · nH₂O and ZrO₂ is analyzed. The phase composition, crystallite size, porous structure and agglomeration during neutralization are studied by a complex of physicochemical methods to establish the formation mechanism, and to assess the possibility of obtaining ZrO₂ with the required porous structure. The obtained results and the formation mechanism are discussed from the point of view of non-classical concepts of nucleation and crystal growth.

2. Experimental

2.1. Synthesis technique

A 0.2 M ZrOCl_2 solution was used as the initial solution. For this, 25.78 g of $\text{ZrOCl}_2 \cdot 8\text{H}_2\text{O}$ was dissolved in 200 ml of doubly distilled water and the volume of the solution was brought to 400 ml ($\rho = 1.027 \text{ g/cm}^3$). The hydrolysis was carried out in a three-necked borosilicate glass flask in a batch mode (8 h at $(100 \pm 1)^\circ\text{C}$ – 16 h at room temperature). The timing began when the solution temperature reached 95°C . Sol samples with a volume of 95 ml were taken after 36 ± 2 and 61 ± 3 h. The final hydrolysis time of the remaining sol was 126 ± 4 h. The resulting sols were neutralized by adding a 13 M ammonia solution ($\rho = 0.909 \text{ g/cm}^3$ at 20°C) to $\text{pH} = 9.1$. The preparation of $\text{ZrO}_2 \cdot n\text{H}_2\text{O}$ by direct precipitation from a 0.6 M ZrOCl_2 solution with a 13 M ammonia solution is described in [1].

Then the mother liquor was vacuum filtered using a Buchner funnel. The resulting mass was washed via decantation until there was no Cl^- ($\sim 0.2 \text{ L H}_2\text{O} / \text{g ZrO}_2$, controlled with 0.1 N AgNO_3). After washing, the mother liquor was squeezed out, and the resulting mass was dried for 4 h at 60°C and 1 h at 90°C . To study the pore structure and phase composition of ZrO_2 , the $\text{ZrO}_2 \cdot n\text{H}_2\text{O}$ samples were subjected to thermal treatment in a muffle furnace in the stepwise mode of 170°C , 0.5 h; 250°C , 0.5 h; $300 - 500^\circ\text{C}$, 0.5 h. The temperature growth rate was 4°C/min . The samples are denoted as $\text{ZrO}_2\text{-}P/H(x)\text{-}y$, where P – precipitation method, $H(x)$ – hydrolysis method and its duration, h , y – treatment temperature, $^\circ\text{C}$.

2.2. Characterization methods

Synchronous thermal analysis of $\text{ZrO}_2 \cdot n\text{H}_2\text{O}$ samples was conducted on a Shimadzu DTG-60A thermal analyzer. The weighed portion of a sample was 16 – 20 mg; the material of the crucibles and the reference was corundum; the heating rate was 10°C/min . The heat of crystallization data was used to determine the proportion of ZrO_2 that passed into the solid phase as a result of hydrolysis:

$$a_H = \left(1 - \frac{\Delta Q(\text{ZrO}_2 - H(x))}{\Delta Q(\text{ZrO}_2 - P)} \times 100\% \right). \quad (2)$$

Characteristics of the pore structure of $\text{ZrO}_2 \cdot n\text{H}_2\text{O}$ and ZrO_2 were identified via the low-temperature sorption of N_2 on a Quantachrome Autosorb 6iSA instrument at 77 K. Before analysis, the samples were degassed in vacuum for 1 h at 100°C (for $\text{ZrO}_2 \cdot n\text{H}_2\text{O}$) or 250°C (for ZrO_2). Specific surface area (S_{BET} , m^2/g) was calculated using the Brunauer–Emmett–Teller (BET) technique; total pore volume (V_Σ , cm^3/g) was determined from the limiting value of absorbed N_2 at $p/p_0 = 0.97$; pore size distribution was calculated according to the density functional theory [14].

The phase composition and crystalline size of the ZrO_2 samples were studied by powder X-ray diffraction on a Shimadzu XRD-6100 diffractometer (Cu anode, Ni filter) using D:S:R = $0.5^\circ : 0.5^\circ : 0.15 \text{ mm}$ slits in the step of 0.02° with an acquisition time of 3 s per point. The volume fraction of the tetragonal phase ($t\text{-ZrO}_2$, V_t , vol.%) was calculated as described in [15]. The Scherrer equation ($K = 0.94$; $\lambda(\text{CuK}\alpha_1) = 0.15406 \text{ nm}$) was used to calculate the crystalline size of $t\text{-ZrO}_2$ (d_t , nm) and $m\text{-ZrO}_2$ (d_m , nm).

The size distribution of particles in the as-synthesized $\text{ZrO}_2 \cdot n\text{H}_2\text{O}$ sols and colloidal suspensions were investigated by laser diffraction (LD) on a “Shimadzu SALD-2300” particle size analyzer. For this, colloidal suspensions of the samples were prepared by mixing 80 mg of the product with 250 mL of distilled water and sonicating the mixture for 3 min by a 700 W ultrasonic disperser. The Refractive index was 1.85.

3. Results and discussion

3.1. Simultaneous TG-DTA

Fig. 1 and Table 1 shows results from simultaneous thermal analysis of $\text{ZrO}_2 \cdot n\text{H}_2\text{O}$ samples. Two regions can be distinguished from the differential thermal curves.

In the first region ($20 - 300^\circ\text{C}$), $\text{ZrO}_2 \cdot n\text{H}_2\text{O}$ underwent two steps of dehydration: the desorption of unbound water (Δm_1) and the removal of structural water during the thermal decomposition of oxyhydroxide (Δm_2) [16]. An increase in the hydrolysis duration leads to a non-monotonic increase in the amount of structural water and the total amount of water n (Table 1). Wherein the content of unbound water changes insignificantly. The $\text{ZrO}_2\text{-H}(36)$ sample has the highest hydration, and the $\text{ZrO}_2\text{-H}(126)$ sample has the lowest.

Crystallization of X-ray amorphous ZrO_2 ($a\text{-ZrO}_2$) obtained after dehydration of $\text{ZrO}_2 \cdot n\text{H}_2\text{O}$ occurs in the second region ($370 - 470^\circ\text{C}$). Here, weight loss (Δm_3) is also observed, which does not depend on the hydrolysis duration. The $\text{ZrO}_2\text{-P}$ sample obtained by precipitation is characterized by the maximum heat of crystallization of $a\text{-ZrO}_2$ (ΔQ). The crystallization peak of $a\text{-ZrO}_2$ for the $\text{ZrO}_2\text{-H}(126)$ sample is insignificant. The ΔQ value and the crystallization onset temperature (T_{init}) decrease with increasing the hydrolysis duration (Table 1). This regularity indicates an increase in the content of the hydrolysis product and, accordingly, a decrease in the content of $a\text{-ZrO}_2 \cdot n\text{H}_2\text{O}$, formed

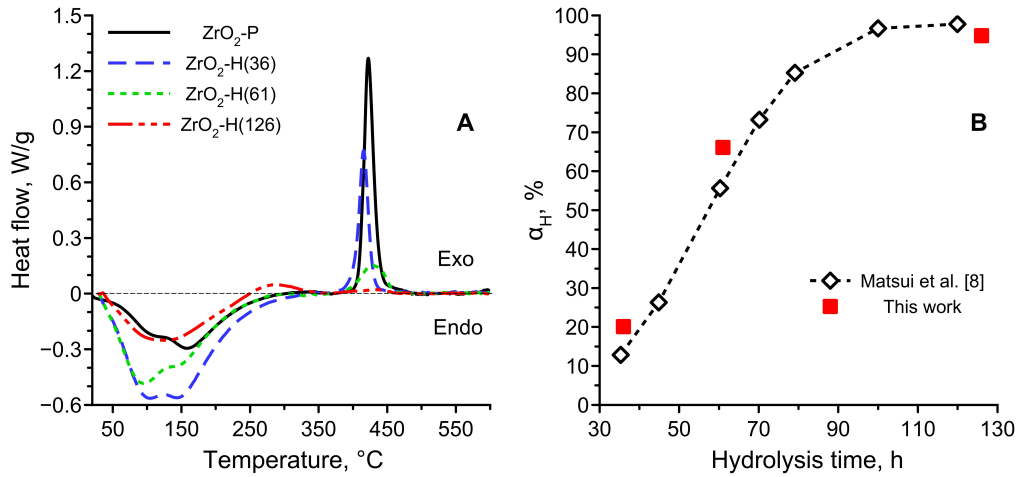


FIG. 1. DT-curves of samples (A) and results of determining the fraction of hydrolyzed zirconia

TABLE 1. Results from the simultaneous TG-DTA of $ZrO_2 \cdot nH_2O$

Sample	nH_2O^*	Weight loss, wt%			α - ZrO_2 crystallization	
		Δm_1	Δm_2	Δm_3	ΔQ , J/g ZrO_2	T_{init} , °C
		20 – 125 °C	125 – 300 °C	300 – 800 °C		
ZrO ₂ -P	1.16	2.4	9.7	2.4	130	411
ZrO ₂ -H(36)	1.54	3.6	11.6	3.2	102	402
ZrO ₂ -H(61)	1.20	4.0	7.4	3.4	43	397
ZrO ₂ -H(126)	0.80	2.1	5.2	3.2	~ 7	–

$$*n = \frac{6.85 \cdot \Delta m}{100 - \Delta m}, \text{ where } \Delta m - \text{total weight loss, wt\%}$$

during the neutralization of partially hydrolyzed solutions. The change in the heat of crystallization made it possible to estimate the amount of $ZrO_2 \cdot nH_2O$ (α_H) formed during complete hydrolysis (Fig. 1B). Comparison with the results [6–9], which determined α_H by chelation titration, shows a similar dependence and close absolute values of α_H .

3.2. Powder X-Ray diffraction

The results of X-ray diffraction are shown in Fig. 2 and Table 2. The ZrO₂-P sample obtained by precipitation is characterized by an X-ray amorphous state, which corresponds to the halo (Fig. 2A). The content of the poorly crystallized m -ZrO₂ phase in the resulting precipitates increased with longer hydrolysis durations. The formation of a mixture of m -ZrO₂ · nH_2O and α -ZrO₂ · nH_2O (hydrolysis duration of 36 and 61 h) was associated with the partial formation of m -ZrO₂ during hydrolysis of ZrOCl₂, as well as the precipitation from residual ZrOCl₂ upon neutralization with an ammonia solution, respectively. This was consistent with the results of TG-DTA: the content of the crystalline m -ZrO₂ increases with lengthening the hydrolysis duration. The crystallite size (coherent scattering region) of m -ZrO₂ increased with the hydrolysis duration reaching 3.4 nm (Table 2) upon hydrolysis for 126 h, which was consistent with prior results [8].

Significant changes in the phase composition and crystallite size of the ZrO₂-P sample occurred after thermal treatment at 450 °C, which corresponds to the completion of the α -ZrO₂ crystallization: a mixture of t - and m -ZrO₂ is formed with a predominance of t -ZrO₂ (Fig. 2B). The fraction of m -ZrO₂ increased, and the size of the crystallites of m -ZrO₂ and t -ZrO₂ decreased with longer hydrolysis times in the samples thermally-treated at 450 °C (Table 2).

The formation of metastable t -ZrO₂ during crystallization and its further polymorphic transformation into m -ZrO₂ is explained by the structural similarity of α -ZrO₂ and t -ZrO₂ [17], and the achievement of the critical crystallite size of about 30 nm, previously obtained [18] based on thermodynamic considerations about the influence of surface energy, respectively. However, the critical size of the t -ZrO₂ crystallite depends on the conditions of synthesis, and subsequent processing of ZrO₂ and can be much less than 30 nm [19]. The crystallite size of t -ZrO₂ is different for

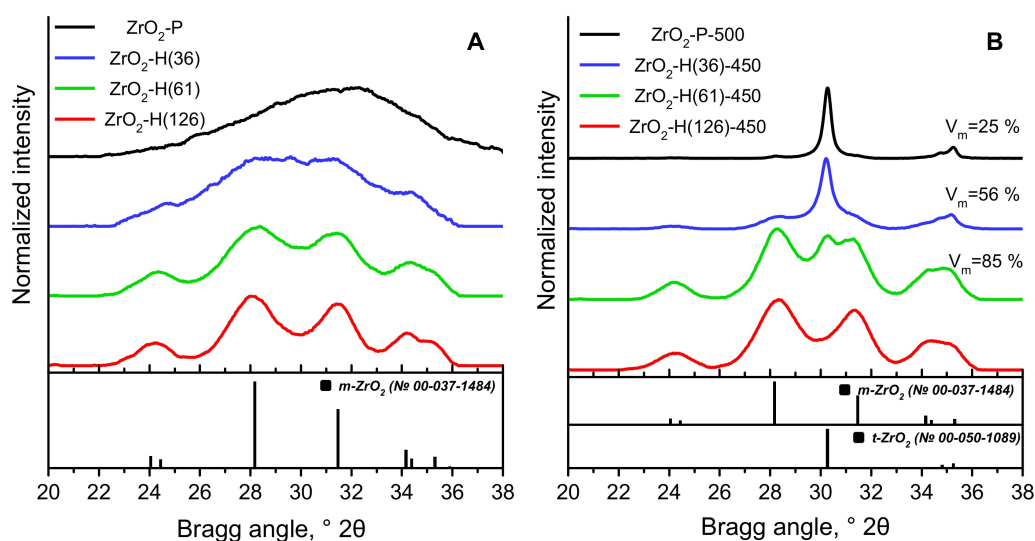


FIG. 2. XRD results of the as-prepared (A) and thermal treatment samples (B)

TABLE 2. *m*-ZrO₂ crystalline size (d_t given in parentheses)

Hydrolysis duration, h	Thermal treatment, °C					
	100	300	350	450	500	600
0 (precipitation)	< 2	–	–	–	13.9 (24.1)	–
36	2.1	–	3.6	5.3 (14.4)	–	–
61	3.1	–	3.9	5.5 (8.3)	–	–
126	3.4	3.7	3.8	4.2	4.4	5.8

samples that differ in the duration of hydrolysis and heat-treated at 450 – 500 °C (Table 2). The imposition of the kinetic factor proposed in [20], namely, only a part of the crystallites with a size above a critical value pass into a new phase, explain the observed decrease in d_t . The formation of *m*-ZrO₂ crystallites smaller than *t*-ZrO₂ can be explained by twinning [21].

An increase in the treatment temperature of ZrO₂-H(126) leads to a gradual increase in the size of *m*-ZrO₂ crystallites (Table 2). A noticeable change in d_m begins to occur at $T \geq 300^\circ\text{C}$, and a sharp increase occurs at 600 °C. After crystallization of *a*-ZrO₂, a stronger increase in the size of *m*-ZrO₂ crystallites occurs than with an increase in temperature from 100 to 350 °C in the case of samples with an intermediate duration of hydrolysis. This is due to the contribution of the *t*-ZrO₂ → *m*-ZrO₂ transition, which results in the formation of larger *m*-ZrO₂ crystallites.

4. Porous structure

The results of studying the texture of samples by the N₂ physisorption method are shown in Fig. 3 and Fig. 4. The isotherm for the ZrO₂-P-500 sample obtained by precipitation belongs to type IVa with an H4 hysteresis loop, which corresponds to a mesoporous structure according to IUPAC [14]. The contribution of the type I isotherm on the isotherms of the corresponding thermally treated samples increases with lengthening the hydrolysis duration. In this case, the hysteresis loops are retained and the contribution of the type IVa isotherm is present. The listed characteristics of the isotherms indicate the presence of micro- and mesopores in the texture of the samples. For the ZrO₂-H(61)-500 sample, a change in the type of hysteresis to H3 is observed, and for which it can be assumed that the pores are formed by aggregates of plot-like particles. In samples ZrO₂-H(126)-300 and ZrO₂-H(126)-500, the hysteresis loops are small; therefore, the texture is mainly represented by micropores.

The conclusions based on the isotherms are confirmed by the results of calculating the pore size distribution curves. Samples ZrO₂-P-500 and ZrO₂-H(36)-500, in the preparation of which the precipitation product predominated, are represented by small mesopores 2 – 10 nm. The proportion of micropores simultaneously increases with the

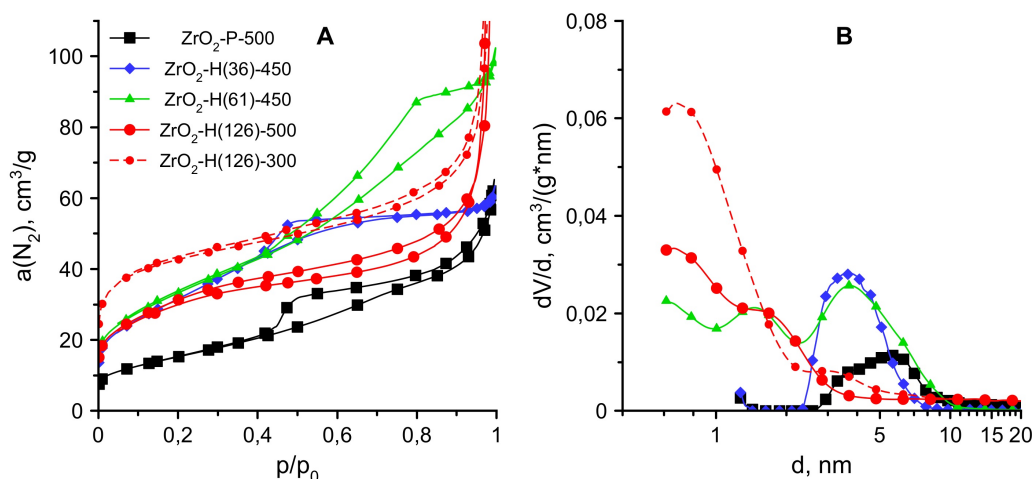


FIG. 3. N_2 physisorption isotherms (A) and pore size distribution (B) for ZrO_2 samples

contribution of hydrolysis to the formation of ZrO_2 (samples $ZrO_2-H(126)-300$ and $ZrO_2-H(126)-500$). The absorption of a large amount of nitrogen at $p/p_0 > 0.97$ is a feature of the sorption isotherms of the $ZrO_2-H(126)-300$ and $ZrO_2-H(126)-500$ samples. The corresponding pore size distribution curves show nonzero dV/d values at diameters greater than 5 nm (Fig. 3B) and the presence of a local maximum at 70 nm (not shown here). This may be due to the presence of secondary porosity formed by the gap between agglomerates (secondary particles).

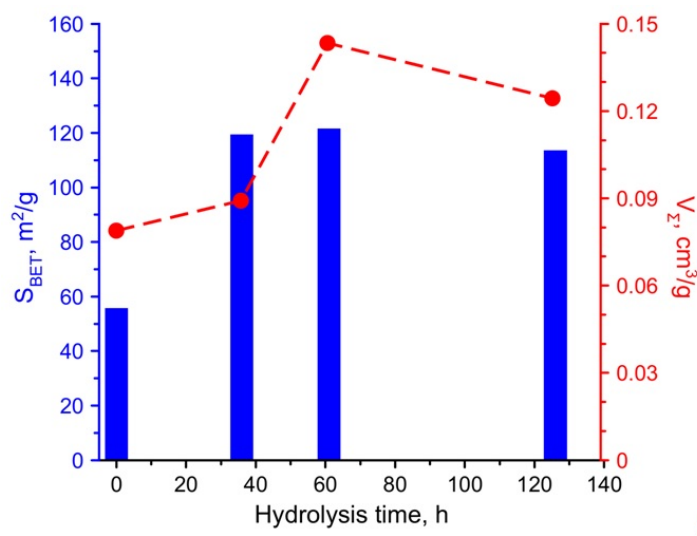


FIG. 4. Dependence of specific surface area and total pore volume vs hydrolysis duration for thermal treatment at 450 – 500 °C samples

The specific surface area of ZrO_2 increases with lengthening the hydrolysis duration (Fig. 4). A similar dependence is observed for V_Σ at $p/p_0 = 0.97$. The specific surface area of the $ZrO_2-H(126)$ sample obtained by complete hydrolysis decreases from 156 to 113 m^2/g , and the total pore volume from 0.149 to 0.124 cm^3/g with an increase in the treatment temperature from 300 to 500 °C. High S_{BET} and V_Σ correspond to loose packing of crystallites. The appearance in the phase composition of an amount of $m-ZrO_2$ comparable to the amount of $t-ZrO_2$ (sample $ZrO_2-H(36)-450$), and reduced size of $t-ZrO_2$ crystallites contribute to a noticeable increase in S_{BET} with lengthening the hydrolysis duration from 0 to 36 h (samples $ZrO_2-P-500$ and $ZrO_2-H(36)-450$, respectively). Poorly crystallized $m-ZrO_2$, which has a high S_{BET} (sample $ZrO_2-H(126)-450$), begins to make a greater contribution to S_{BET} with a further increase in the duration of hydrolysis to 61 h. The obtained S_{BET} values of $ZrO_2-H(36)-450$ and $ZrO_2-H(61)-450$ exceed the sum of S_{BET} of individual $t-ZrO_2$ and $m-ZrO_2$ samples $ZrO_2-P-500$ and $ZrO_2-H(126)-450$, respectively, taking into account their share in the phase composition.

There is an inverse proportionality between the crystallite size of the phases and S_{BET} according to the ratio:

$$d_{Ads} = \frac{A}{S_{BET} \times \rho}, \quad (3)$$

where ρ – density, A – coefficient depending on the shape of the crystallites. The calculation of d_{Ads} according to formula (3) and data on S_{BET} taking into account the density of the predominant phase (6.134 g/cm^3 for $t\text{-ZrO}_2$ and 5.817 g/cm^3 for $m\text{-ZrO}_2$) for different morphologies of particles ($A = 6$ for spherical, $A = 4$ for rod-shaped and $A = 2$ for plate-like particles) showed that d_{Ads} values closest to d_{XRD} for samples with a predominance of $m\text{-ZrO}_2$ are achieved under the assumption of a plate-like or rod-shaped particle and in the case of the predominance of $t\text{-ZrO}_2$ assuming a spherical shape (Table 3). The order of the d_{XRD} and d_{Ads} values is the same. Consequently, the specific surface area calculated from the N_2 sorption data is determined precisely by crystallites, and the formation of larger agglomerates and aggregates does not affect its value. It should be noted that the initial non-heat treated $ZrO_2\text{-P}$ sample with $S_{BET} = 231 \text{ m}^2/\text{g}$ has an equivalent particle size of 1.8 nm in the approximation of lamellar morphology ($\rho = 4.86 \text{ g/cm}^3$ [22]), which corresponds to the PXRD result on its X-ray amorphous state (Table 2).

TABLE 3. Particle size d_{SSA} values calculated using equation (3)

Sample	$d_{Ads} (A = 6)$, nm	$d_{Ads} (A = 4)$, nm	$d_{Ads} (A = 2)$, nm
ZrO ₂ -P	5.3	3.6	1.8
ZrO ₂ -P-500	17.5	11.6	5.8
ZrO ₂ -H36-450	8.2	5.4	2.7
ZrO ₂ -H61-450	8.5	5.6	2.8
ZrO ₂ -H126-300	6.6	4.4	2.2
ZrO ₂ -H126-500	9.1	6.1	3.0

5. Laser diffraction

The resulting dispersed systems visually differed in sedimentation and coagulation stability. The $ZrO_2 \cdot nH_2O$ sol obtained by hydrolysis of a $ZrOCl_2$ solution for 126 h (ZrO₂-H(126) sol, Fig. 5) was characterized by a small size of secondary particles (agglomerates 210 nm) and a narrow size distribution. The sol of this sample was characterized by sedimentation and coagulation stability since noticeable signs of sedimentation were detected after several days, and ultrasonic treatment did not affect the given distribution. The results of laser diffraction for the ZrO₂-H(126) sol agreed with the results [6], where the TEM method showed the formation of agglomerates with a size of 170 nm upon hydrolysis of a 0.2 M $ZrOCl_2$ solution. For the sol obtained after 36 h of hydrolysis, the distributions could not be measured due to the low concentration of particles, while for the sol obtained after 61 h of hydrolysis, the distributions differ little from the distribution for ZrO₂-H(126), and the mean diameter was 0.20 μm . Active coagulation of the primary parts with the formation of nanoscale agglomerates occurred during the first 60 h of hydrolysis, at which 60% conversion of $ZrOCl_2$ to $m\text{-ZrO}_2 \cdot nH_2O$ was achieved. The obtained results partially agree with the results [23, 24], where it was shown by the DLS method that active growth of agglomerates was observed in the first 30 – 40 h of hydrolysis, and the time interval decreased to ~ 20 h with an increase in the initial concentration of the $ZrOCl_2$ solution.

Neutralization of the resulting sol with an ammonia solution is a common technique [5, 25], which makes it possible to simplify the subsequent washing of the precipitate from Cl^- and separation from the mother liquor. The addition of ammonia promotes additional coagulation of the sol, the formation of aggregates larger by an order (ZrO₂-H(126) suspension, Fig. 5), and the appearance of a bimodal distribution. The lack of coagulation stability of the ZrO₂-H(126) suspension led to a gradual coarsening of the aggregates, and the size distribution became close to that of the ZrO₂-P suspension. The aggregates of particles of the sample obtained by direct precipitation (ZrO₂-P suspension, Fig. 5) had an even larger size and retained a bimodal distribution.

6. Formation mechanism

According to [26, 27], during the dissolution of $ZrOCl_2$ because of hydrolysis and primary polymerization, zirconium is in solution mainly in two forms, between which there is a mobile equilibrium depending on pH: $[Zr_4(OH)_8(H_2O)_{16}]^{8+}$ and $[Zr_8(OH)_{20}(H_2O)_{24}]^{12+}$. The 0.2 M $ZrOCl_2$ solution used in this work had a pH equal to

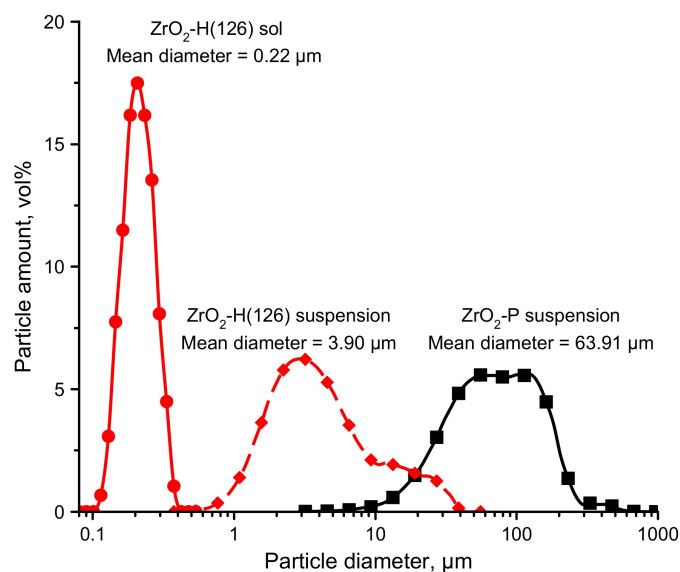


FIG. 5. Agglomerate and aggregate size distribution of the sol and suspensions

0.9 and 0.5 at 20 and 90 °C, respectively, which indicates the predominant presence of zirconium in $[\text{Zr}_4(\text{OH})_8(\text{H}_2\text{O})_{16}]^{8+}$ form. The pH of the resulting suspensions after 36, 61, and 126 h of hydrolysis was 0.4 – 0.5 at 20 °C. Consequently, the form $[\text{Zr}_4(\text{OH})_8(\text{H}_2\text{O})_{16}]^{8+}$ predominated at any time of hydrolysis.

The above data shows the following. X-ray amorphous $\text{ZrO}_2 \cdot n\text{H}_2\text{O}$ is formed during direct precipitation from a ZrOCl_2 solution and characterized by a plot-like morphology of primary particles, which are randomly folded into larger agglomerates and aggregates resulting from rapid coagulation. $\text{ZrO}_2 \cdot n\text{H}_2\text{O}$ crystallizes upon further heat treatment with the formation of predominantly *t*- ZrO_2 due to the inheritance of the structure of primary nanometer particles in $\text{ZrO}_2 \cdot n\text{H}_2\text{O}$, and the morphology of *t*- ZrO_2 crystallites is close to spherical. The porous structure is represented by micropores in *a*- $\text{ZrO}_2 \cdot n\text{H}_2\text{O}$ and mesopores in *t*- ZrO_2 .

Long-term hydrolysis of the ZrOCl_2 solution at 100 °C led to the formation of *m*- $\text{ZrO}_2 \cdot n\text{H}_2\text{O}$. A mixture of crystalline *m*- $\text{ZrO}_2 \cdot n\text{H}_2\text{O}$ and *a*- $\text{ZrO}_2 \cdot n\text{H}_2\text{O}$ with a predominance of the latter was formed after 36 h of hydrolysis and subsequent neutralization of the resulting sol with an ammonia solution. Monoclinic and tetragonal zirconia, respectively, were formed due to dehydration and crystallization during subsequent thermal treatment, and their ratio depends on the ratio of *m*- $\text{ZrO}_2 \cdot n\text{H}_2\text{O}$ and *a*- $\text{ZrO}_2 \cdot n\text{H}_2\text{O}$ in the initial precipitates. The observed excess of the content of *m*- ZrO_2 after heat treatment relative to its content in untreated mixtures of *m*- $\text{ZrO}_2 \cdot n\text{H}_2\text{O}$ and *a*- $\text{ZrO}_2 \cdot n\text{H}_2\text{O}$ maybe since *m*- ZrO_2 from *m*- $\text{ZrO}_2 \cdot n\text{H}_2\text{O}$ is a nucleus for the growth of new crystallites of *m*- ZrO_2 from *a*- $\text{ZrO}_2 \cdot n\text{H}_2\text{O}$ or accelerating the transition *t*- ZrO_2 to *m*- ZrO_2 [28].

The increased hydration of the $\text{ZrO}_2\text{-H}(36)$ sample detected by the TG-DTA method was associated with the fact that in the first 36 h of hydrolysis, the polymerization of $[\text{Zr}_4(\text{OH})_8(\text{H}_2\text{O})_{16}]^{8+}$ proceeded with the formation of a larger size polymer cluster and increased content of (OH) and (H₂O) due to olation and oxolation. A similar explanation for the induction period was suggested by Hu et al. [24] based on the results of a study of thermohydrolytic polymerization of a ZrOCl_2 solution by the SAXS method. An increase in the duration of hydrolysis led to the consumption of $[\text{Zr}_4(\text{OH})_8(\text{H}_2\text{O})_{16}]^{8+}$ and its oligomers for the growth of *m*- ZrO_2 crystallites, and a regular decrease in the hydration of the resulting product. The main growth of *m*- ZrO_2 crystallites occurred in the period from 36 to 61 h (Table 2), and the maximum CSR value was 3.4 nm. This stage is limiting. The addition of a base in the synthesis by direct precipitation seems to greatly accelerate the passage of the above steps. As a result, the olation and oxolation with the formation of oligomers are less deep, which determines the X-ray amorphous nature of the precipitation product.

The growth of agglomerates 100 – 300 nm proceeds in parallel with the process of crystallite growth. The size of the agglomerates did not change after 61 h of hydrolysis. Agglomerates were composed of plot-like and/or rod-shaped nanocrystallites of *m*- ZrO_2 and have a microporous structure. These results for the morphology of aggregates confirm the prior results of TEM by other authors [7, 24]. The plot-like and/or rod-shaped morphology of *m*- ZrO_2 particles indicated an oriented attachment of crystallites [29].

The final scheme of the sequence of the formation of $\text{ZrO}_2 \cdot n\text{H}_2\text{O}$ during hydrolysis and precipitation based on the data of this work is shown in Fig. 6.

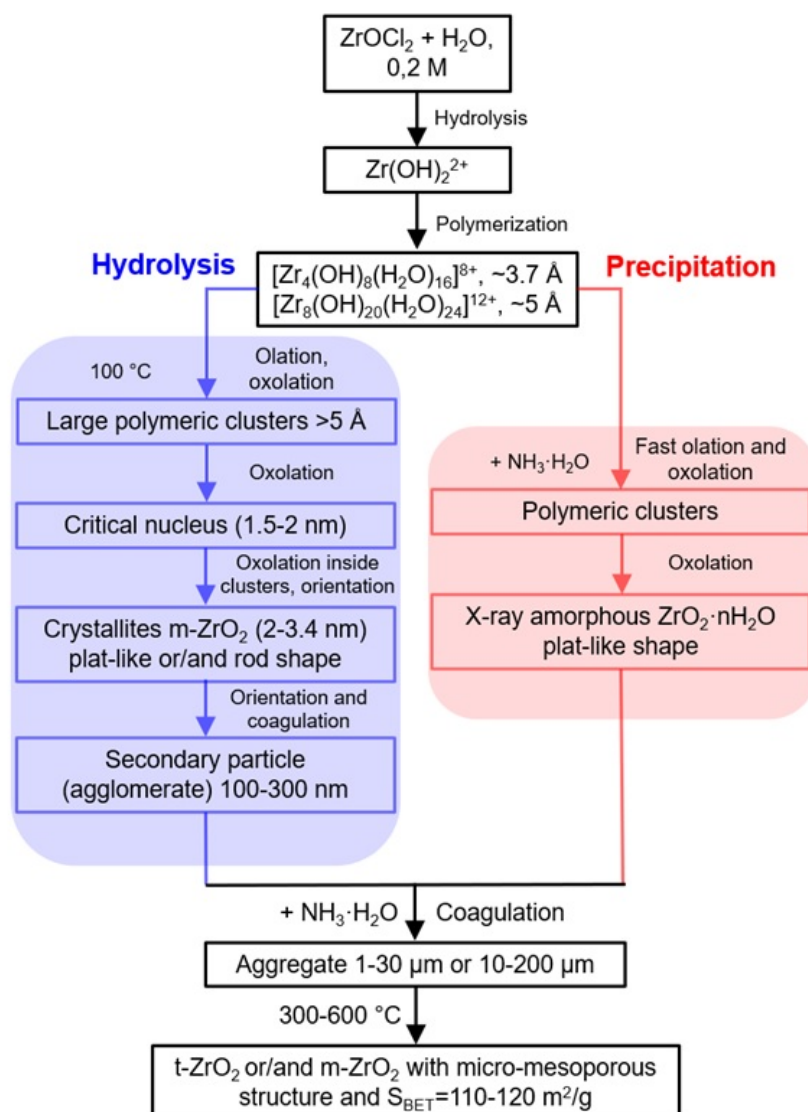


FIG. 6. Formation mechanism of $\text{ZrO}_2 \cdot n\text{H}_2\text{O}$ during hydrolysis and precipitation

The presence of polymeric zirconium hydroxocomplexes in the initial solution does not allow one to consider the formation of $\text{ZrO}_2 \cdot n\text{H}_2\text{O}$ within the framework of the classical theory of crystal growth. Comparison of the stages in Fig. 6 with nonclassical mechanisms of nucleation and growth of crystals shows that the formation of $m\text{-ZrO}_2$ during hydrolysis is the closest to the mechanism of aggregation nucleation [28]. Comparison of XRD data and adsorption-structural analysis indicated that the size of the $m\text{-ZrO}_2$ nucleus is in the range of 1.5 – 2 nm, which is 4 – 6 times greater than the gyration radius of the dominant $[\text{Zr}_4(\text{OH})_8(\text{H}_2\text{O})_{16}]^{8+}$ ($R_g = 3.7 \text{ \AA}$ [24, 27]). Rapid crystallite growth begins when the size of the $m\text{-ZrO}_2$ crystallite reaches 2.1 nm after 36 h of hydrolysis, and this value is the upper limit. The lower value depends on the size of the oligomers formed from $[\text{Zr}_4(\text{OH})_8(\text{H}_2\text{O})_{16}]^{8+}$ and its exact experimental determination by the used methods is impossible. The same range of possible critical nucleus size includes the equivalent particle size in $a\text{-ZrO}_2 \cdot n\text{H}_2\text{O}$ equal to 1.8 nm.

7. Conclusion

As a result of the work, the phase formation, texture, and morphology of $\text{ZrO}_2 \cdot n\text{H}_2\text{O}$ and ZrO_2 were studied depending on the hydrolysis duration of the ZrOCl_2 solution followed by neutralization of the sol. It was found that the above characteristics strongly depend on the completeness of the hydrolysis of ZrOCl_2 with the formation of poorly crystallized $m\text{-ZrO}_2$. The properties of $\text{ZrO}_2 \cdot n\text{H}_2\text{O}$ and the corresponding ZrO_2 obtained by hydrolysis are very different from the properties of $\text{ZrO}_2 \cdot n\text{H}_2\text{O}$ and the corresponding ZrO_2 obtained by direct precipitation, which is

due to the differences in the number of stages by which the formation of $ZrO_2 \cdot nH_2O$ occurs. The size of the critical nucleus was estimated. An important practical result was show the possibility of adjusting the ratio of *t*- and *m*- ZrO_2 with a constant high specific surface area exceeding the additive effect of individual *t*- and *m*- ZrO_2 . The possibility of creating a hierarchical porous micro-mesoporous structure was also shown, which is important for the preparation of catalytic materials based on ZrO_2 .

References

- [1] Omarov Sh.O., Pakhomov N.A. Varying the conditions of $ZrO_2 \cdot nH_2O$ precipitation and aging as a way of controlling the phase composition and texture of ZrO_2 . *Catal. Ind.*, 2021, **13**(1), P. 12–20.
- [2] Otroshchenko T., Radnik J., Schneider M., Rodemerck U., Linke D., Kondratenko E.V. Bulk binary ZrO_2 -based oxides as highly active alternative-type catalysts for non-oxidative isobutane dehydrogenation. *Chem. Commun.*, 2016, **52**, P. 8164–8167.
- [3] Omarov Sh.O., Vlasov E.A., et al. Physico-chemical properties of MoO_3/ZrO_2 catalysts prepared by dry mixing for isobutane alkylation and butene transformations. *Appl. Catal. B.*, 2018, **230**, P. 246–259.
- [4] Omarov Sh.O., Sladkovskiy D.A., Martinson K.D., Peurla M., Aho A., Murzin D.Yu., Popkov V.I. Influence of the initial state of ZrO_2 on genesis, activity and stability of Ni/ZrO_2 catalysts for steam reforming of glycerol. *Appl. Catal. A*, 2021, **616**, P. 118098.
- [5] Li J., Chen J., Song W., Liu J., Shen W. Influence of zirconia crystal phase on the catalytic performance of Au/ZrO_2 catalysts for low-temperature water-gas shift reaction. *Appl. Catal. A*, 2008, **334**, P. 321–329.
- [6] Matsui K., Ohga M. Formation mechanism of hydrous zirconia particles produced by the hydrolysis of $ZrOCl_2$ solutions. *J. Am. Ceram. Soc.*, 1997, **80**(8), P. 1949–1956.
- [7] Matsui K., Ohga M. formation mechanism of hydrous zirconia particles produced by the hydrolysis of $ZrOCl_2$ solutions: II. *J. Am. Ceram. Soc.*, 2000, **83**(6), P. 1389–1392.
- [8] Matsui K., Ohga M. Formation mechanism of hydrous zirconia particles produced by the hydrolysis of $ZrOCl_2$ solutions: III, kinetics study for the nucleation and crystal-growth processes of primary particles. *J. Am. Ceram. Soc.*, 2001, **84**(10), P. 2302–2012.
- [9] Matsui K., Ohga M. Formation mechanism of hydrous zirconia particles produced by the hydrolysis of $ZrOCl_2$ solutions: IV, effect of $ZrOCl_2$ concentration and reaction temperature. *J. Am. Ceram. Soc.*, 2002, **85**(3), P. 545–553.
- [10] Sharikov F.Yu., Almjashveva O.V., Gusarov V.V. Thermal analysis of formation of ZrO_2 nanoparticles under hydrothermal conditions. *Russ. J. Inorg. Chem.*, 2006, **51**(10), P. 1538–1542.
- [11] Raghavendra V.B., Naik S., Antony M., Ramalingam G., Rajamathi M., Raghavan S. Amorphous, monoclinic, and tetragonal porous zirconia through a controlled self-sustained combustion route. *J. Am. Ceram. Soc.*, 2011, **94**(6), P. 1747–1755.
- [12] Štefanić G., Musić S., Popović S., Furić K. Formation of ZrO_2 by the thermal decomposition of zirconium salts. *Croat. Chem. Acta.*, 1996, **69**, P. 223–239.
- [13] Zhukov A.V., Chizhevskaya S.V., Phyo P., Panov V.A. Heterophase synthesis of zirconium hydroxide from zirconium oxychloride. *Inorg. Mater.*, 2019, **55**(10), P. 994–1000.
- [14] Thommes M., Kaneko K., et al. Physisorption of gases, with special reference to the evaluation of surface area and pore size distribution (IUPAC Technical Report). *Pure Appl. Chem.*, 2015, **87**(9-10), P. 1051–1069.
- [15] Toraya H., Yoshimura M., Somiya S. Calibration curve for quantitative analysis of the monoclinic tetragonal ZrO_2 system by X-ray diffraction. *J. Am. Chem. Soc.*, 1984, **67**(6), P. C119–C121.
- [16] Sato T. The thermal decomposition of zirconium oxyhydroxide. *J. Therm. Anal. Calorim.*, 2002, **69**, P. 255–265.
- [17] Livage J., Doi K., Mazires C. Nature and thermal evolution of amorphous hydrated zirconium oxide. *J. Am. Ceram. Soc.*, 1968, **51**(6), P. 349–353.
- [18] Garvie R.C. The occurrence of metastable tetragonal zirconia as a crystallite size effect. *J. Phys. Chem.*, 1965, **69**(4), P. 1238–1243.
- [19] Almjashveva O.V., Lomanova N.A., Popkov V.I., Proskurina O.V., Tugova E.A., Gusarov V.V. The minimum size of oxide nanocrystals: phenomenological thermodynamic vs crystal-chemical approaches. *Nanosystems: Physics, Chemistry, Mathematics*, 2019, **10**(4), P. 428–437.
- [20] Mercera P.D.L., Van Ommen J.G., Doesburg E.B.M., Burggraaf A.J., Ross J.R.H. Zirconia as a support for catalysts. Evolution of the texture and structure on calcination in air. *Appl. Catal.*, 1990, **57**, P. 127–148.
- [21] Srinivasan R., Rice L., Davis B.H. Critical particle size and phase transformation in zirconia: transmission electron microscopy and X-ray diffraction studies. *J. Am. Ceram. Soc.*, 1990, **73**(11), P. 3528–3530.
- [22] Ceresoli D., Vanderbilt D. Structural and dielectric properties of amorphous ZrO_2 and HfO_2 . *Phys. Rev. B.*, 2006, **74**(12), P. 125108.
- [23] Hu M. Z.-C., Harris M.T., Byers C.H. Nucleation and growth for synthesis of nanometric zirconia particles by forced hydrolysis. *J. Coll. Int. Sci.*, 1998, **198**, P. 87–99.
- [24] Hu M. Z.-C., Zielke J.T., Byers C.H. Small-angle x-ray scattering studies of early-stage colloid formation by thermohydrolytic polymerization of aqueous zirconyl salt solutions. *J. Mater. Res.*, 1999, **14**(1), P. 103–113.
- [25] Zhao Y., Li W., Zhang M., Tao K. A comparison of surface acidic features between tetragonal and monoclinic nanostructured zirconia. *Catal. Comm.*, 2002, **3**, P. 239–245.
- [26] Clearfield A., Vaughan P.A. The crystal structure of zirconyl chloride octahydrate and zirconyl bromide octahydrate. *Acta Cryst.*, 1956, **9**, P. 555–558.
- [27] Walther C., Rothe J., Fuss M., Büchner S., Koltsov S., Bergmann T. Investigation of polynuclear Zr(IV) hydroxide complexes by nanoelectrospray mass-spectrometry combined with XAFS. *Anal. Bioanal. Chem.*, 2007, **388**, P. 409–431.
- [28] Almjashveva O.V., Gusarov V.V. Metastable clusters and aggregative nucleation mechanism. *Nanosystems: Physics, Chemistry, Mathematics*, 2014, **5**(3), P. 405–416.
- [29] Ivanov V.K., Fedorov P.P., Baranchikov A.Y., Osiko V.V. Oriented attachment of particles: 100 years of investigations of non-classical crystal growth. *Russian Chemical Reviews*, 2014, **83**(12), P. 1204–1222.